Thermal Stability of Lithium Nickel Oxide Derivatives. Part I: $Li_xNi_{1.02}O_2$ and $Li_xNi_{0.89}Al_{0.16}O_2$ ($x = 0.50$ and 0.30)

M. Guilmard, L. Croguennec,* D. Denux, and C. Delmas

Institut de Chimie de la Matière Condensée de Bordeaux CNRS and Ecole Nationale Supérieure de Chimie et Physique de Bordeaux, Université Bordeaux I, 87, Av. Dr A. Schweitzer, 33608 Pessac Cedex, France

Received May 2, 2003. Revised Manuscript Received September 2, 2003

The thermal degradation mechanism of $Li_xNi_{1.02}O_2$ and $Li_xNi_{0.89}Al_{0.16}O_2$ ($x = 0.50$ and 0.30) was studied by in situ X-ray diffraction correlated with thermal gravimetric analysis coupled with mass spectrometry. The degradation mechanism appears to be the same for both types of samples. It consists of two steps: the first step, corresponding to the lamellar to pseudo-spinel transformation, is accompanied by an oxygen loss only for compounds with an initial (Li + M)/O ratio (M = Ni, Al) smaller than $^3/_4$. The second step corresponds to the progressive transformation to a NiO-type structure, with an oxygen loss for both initial lithium compositions. The thermal stabilization obtained by partial aluminum substitution for nickel can be explained by the stability of the Al^{3+} ions in tetrahedral sites, which disrupts the cationic migrations necessary for the phase transformations observed upon increasing temperature to occur.

Introduction

$LiNiO_2$ appears to be a promising positive electrode material for lithium-ion batteries.[1−4] In comparison to $LiCoO_2$, which is presently used in almost all the lithium-ion batteries for portable devices, the main advantages of $LiNiO_2$ are its lower cost and its higher specific energy. However, this material also exhibits some drawbacks, such as its thermal instability in the delithiated state.[5−8] Therefore, improvements are required before $LiNiO_2$ can become competitive in practical devices. Previous studies performed using in-situ X-ray diffraction,[9] thermal gravimetric analyses coupled with mass spectrometry (TGA/MS),[5,10,11] and differential scanning calorimetry (DSC)[6,8,7] have shown that Li_xNiO_2 ($x < 0.50$) converts to a spinel-type phase with an oxygen loss around 200 °C, whereas Li_xCoO_2 ($0.4 < x < 0.6$) is stable until at least 220 °C. $LiCoO_2$ also exhibits a less exothermic decomposition reaction.[5,8] The effect of several cationic substitutions for nickel has been studied in the past few years in an effort to improve the thermal stability of $LiNiO_2$ in its deintercalated state and, thus, cell safety. Partial substitutions of Al,[6] Mn,[12,13] Co,[12,14] Ti,[15,12] or Ti/Mg[16] for nickel were shown by DSC measurements to enhance the thermal stability of delithiated $LiNiO_2$.

In a previous paper,[17] $LiNi_{1-y}Al_yO_2$ ($0.10 \leq y \leq 0.50$) phases synthesized by a coprecipitation method were characterized by X-ray and neutron diffraction. Rietveld refinement analysis showed that for all compounds studied, about 5% extra-nickel ions are present in the interslab space. All experiments described in this paper were conducting starting from either the $Li_{0.95}Ni_{0.89}Al_{0.16}O_2$ or $Li_{0.98}Ni_{1.02}O_2$ phase.[17,18] Charge−discharge cycling of lithium cells with $LiNi_{1-y}Al_yO_2$ as positive electrode material has shown that aluminum substitution suppresses all the phase transitions observed for the $LiNiO_2$ system. Good cycling stability was observed, but the capacity decreased from 125 to 100 mAh/g in the 3−4 V voltage range when the aluminum content was increased from 10 to 25%. The aim of Part I of this

* Corresponding author. Phone: (+33) 5-4000-2234. Fax: (+33) 5-4000-6698. E-mail: crog@icmcb.u-bordeaux.fr.

(1) Dahn, J. R.; Von Sacken, U.; Juzkow, M. W.; Al-Janaby, H. *J. Electrochem. Soc.* **1991**, *138*, 2207.
(2) Broussely, M.; Perton, F.; Labat, J.; Staniewicz, R. J.; Romero, A. *J. Power Sources* **1993**, *43−44*, 209.
(3) Ohzuku, T.; Ueda, A. *Solid State Ionics* **1994**, *69*, 201.
(4) Broussely, M.; Perton, F.; Biensan, P.; Bodet, J. M.; Labat, J.; Lecerf, A.; Delmas, C.; Rougier, A.; Pérès, J. P. *J. Power Sources* **1995**, *54*, 109.
(5) Dahn, J. R.; Fuller, E. W.; Obrovac, M.; Von Sacken, U. *Solid State Ionics* **1994**, *69*, 265.
(6) Ohzuku, T.; Ueda, A.; Kouguchi, M. *J. Electrochem. Soc.* **1995**, *142*, 4033.
(7) Arai, H.; Okada, S.; Sakurai, Y.; Yamaki, J. *Solid State Ionics* **1998**, *109*, 295.
(8) Zhang, Z.; Fouchard, D.; Rea, J. R. *Solid State Ionics* **1998**, *70*, 16.
(9) Thomas, M. G. S. R.; David, W. I. F.; Goodenough, J. B.; Groves, P. *Mater. Res. Bull.* **1985**, *20*, 1137.
(10) Biensan, P.; Simon, B.; Pérès, J. P.; De Guibert, A.; Broussely, M.; Bodet, J. M.; Perton, F. *J. Power Sources* **1999**, *81−82*, 906.
(11) Lee, K.-K.; Yoon, W.-S.; Kim, K.-B.; Lee, K.-Y.; Hong, S.-T. *J. Electrochem. Soc.* **2001**, *148*, A716.
(12) Arai, H.; Okada, S.; Sakurai, Y.; Yamaki, J. *J. Electrochem. Soc.* **1997**, *144*, 3117.
(13) Novak, P.; Nesper, R.; Coluccia, M.; Joho, F.; Piotto Piotto, A. *Extended Abstract of the Lithium Battery Discussion: Electrode Materials*, Arcachon, France, May 27 − June 1; abstract 56.
(14) Cho, J. P.; Jung, H. S.; Park, Y. C.; Kim, G. B.; Lim, H. S. *J. Electrochem.l Soc.* **2000**, *147*, 15.
(15) Chang, S. H.; Kang, S.; Song, S.; Yoon, J.; Choy, J. *Solid State Ionics* **1996**, *86−88*, 171.
(16) Gao, Y.; Yakovleva, M. V.; Ebner, W. B. *Electrochem. Solid-State Lett.* **1998**, *1*, 117.
(17) Guilmard, M.; Rougier, A.; Grüne, M.; Croguennec, L.; Delmas, C. *J. Power Sources* **2002**, *115*, 305.
(18) Delmas, C.; Pérès, J. P.; Rougier, A.; Demourgues, A.; Weill, F.; Chadwick, A.; Broussely, M.; Perton, F.; Biensan, P.; Willmann, P. *J. Power Sources* **1997**, *68*, 120.

10.1021/cm030059f CCC: $25.00
Published on Web 10/22/2003

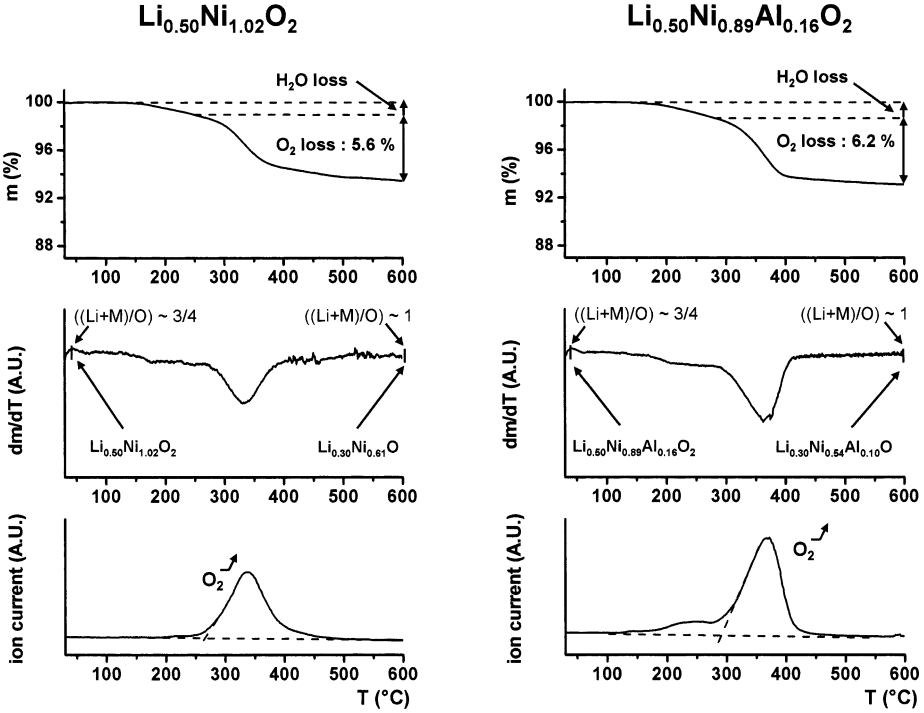

Figure 1. Thermal gravimetric analyses coupled with mass spectrometry for $Li_{0.50}Ni_{1.02}O_2$ and $Li_{0.50}Ni_{0.89}Al_{0.16}O_2$ (sample mass ≈30 mg, heating rate 5 °C/min under an argon stream). The ((Li + M)/O) ratios and chemical compositions are given before and after each oxygen release.

paper is to describe in detail the thermal degradation mechanism of Li_xNiO_2 phases using in situ XRD and TGA/MS results to correlate the oxygen loss with the structural modifications observed upon increasing temperature. Moreover, the effect of aluminum substitution on this mechanism and the origin of its thermal stabilization will also be discussed. In the forthcoming part II, this study will be extended to the $Li_xNi_{0.70}Co_{0.15}Al_{0.15}O_2$ and $Li_xNi_{0.90}Mn_{0.10}O_2$ phases.

Experimental Section

The $Li_xNi_{1.02}O_2$ and $Li_xNi_{0.89}Al_{0.16}O_2$ ($x = 0.30$ or 0.50) phases were obtained by electrochemical lithium deintercalation from $Li_{0.98}Ni_{1.02}O_2$ and $Li_{0.95}Ni_{0.89}Al_{0.16}O_2$, respectively. These starting materials were prepared using the coprecipitation method, as described previously.[17] The electrochemical deintercalation was carried out in Li/liquid electrolyte/positive electrode lithium batteries. The positive electrodes consisted of a mixture of 90 wt % of active material and 10% of carbon black/graphite (1:1); no binder was used, but the positive electrode mixture was pressed in order to provide good electronic contact between the grains and, therefore, to limit cell polarization. $LiPF_6$ (1 M) dissolved in a mixture of propylene carbonate (PC), ethylene carbonate (EC), and dimethyl carbonate (DMC) (1:1:3 by volume) was used as electrolyte. The cells were assembled and charged at room temperature in an argon-filled glovebox; a slow cycling rate (C/200, with C corresponding to a theoretical exchange of one electron in 1 h during charge) was used in galvanostatic mode, with alternate periods of relaxation to maintain the electrochemical reaction close to thermodynamic equilibrium. When charged to the predetermined lithium compositions, the positive electrodes were removed from the cells, washed with DMC, and then dried under vacuum.

Thermal gravimetric analyses coupled with mass spectrometry were carried out under an argon stream, from room temperature to 600 °C, with a heating rate of 5 °C/min. Samples of about 30 mg were used. The X-ray diffraction patterns of the end products were recorded in the 10−80° (2θ) range (0.02°/s) using a Siemens D5000 powder diffractometer with Cu Kα radiation and a graphite diffracted beam monochromator. As only a small amount of powder was available, it was not possible to completely cover the surface of the polycarbonate diffraction sample holder. Therefore, the corresponding XRD patterns exhibit a relatively high background level.

X-ray diffraction patterns were recorded in situ upon increasing temperature by using a capillary furnace on an Inel CPS 120 diffractometer with Co Kα1 radiation. For convenience, all the data presented in this paper will be referred to the Cu Kα1 radiation. The $Li_xNi_{1.02}O_2$ and $Li_xNi_{0.89}Al_{0.16}O_2$ deintercalated phases were introduced in 0.50-mm-diam. capillaries that were sealed and then heated in steps from room temperature to 300 °C at a heating rate of 15 °C/min. At each step, an XRD pattern was recorded over a period of 1 h, after stabilization of the temperature for 10 min.

Large amounts (~200 mg) of the $Li_xNi_{0.89}Al_{0.16}O_2$ deintercalated phases were also heated for 2 h at 200 °C ($Li_{0.30}Ni_{0.89}Al_{0.16}O_2$) or 240 °C ($Li_{0.50}Ni_{0.89}Al_{0.16}O_2$), under a dry argon stream. These samples were characterized ex situ by XRD (Siemens D5000). Step-scan recordings were carried out in the 10−120° (2θ) range (0.02°/40 s), using a sample-holder that prevented any contact of the compound with air.

Scanning electron micrographs were recorded with a Hitachi S4500 field emission microscope with an accelerating voltage of 3.0 kV.

Results

Thermal Analyses by TGA/MS. A comparison of the thermal behavior of the deintercalated $Li_{0.50}Ni_{1.02}O_2$ and $Li_{0.50}Ni_{0.89}Al_{0.16}O_2$ phases was performed using TGA/MS. As shown in Figure 1, no weight loss occurs up to about 150 °C. For both phases, a single peak is observed above 150 °C on the weight loss derivative curves. The gas analyses done using mass spectrometry show that this peak corresponds to oxygen release (Figure 1). Between ca. 150 and 250 °C, a water release associated with desorption of a small amount of CO_2 occurs and appears as a slight weight loss before the oxygen peak.

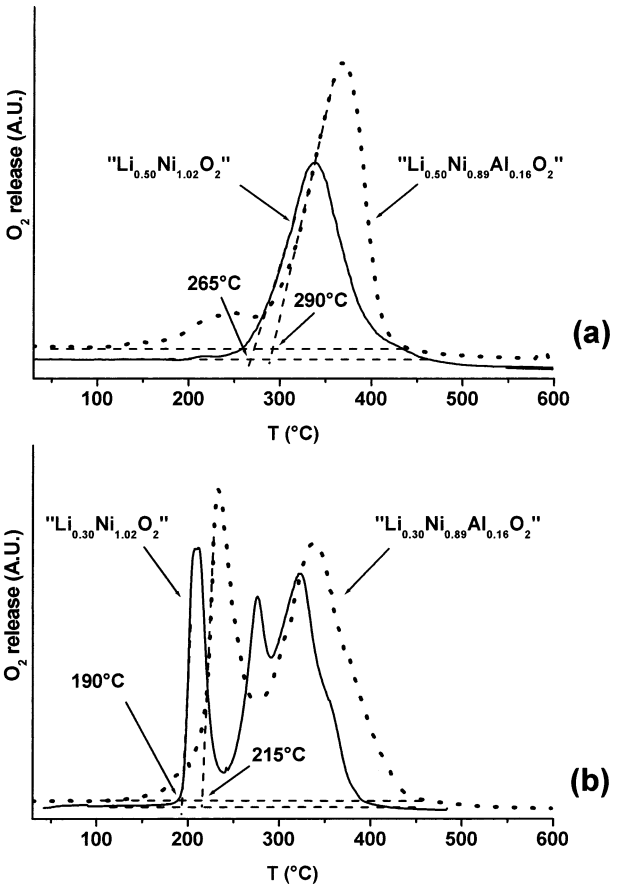

Figure 2. Comparison of oxygen release versus temperature for $Li_xNi_{1.02}O_2$ and $Li_xNi_{0.89}Al_{0.16}O_2$ ($x = 0.50$ (a) and 0.30 (b)) (sample mass ≈30 mg, heating rate 5 °C/min under an argon stream).

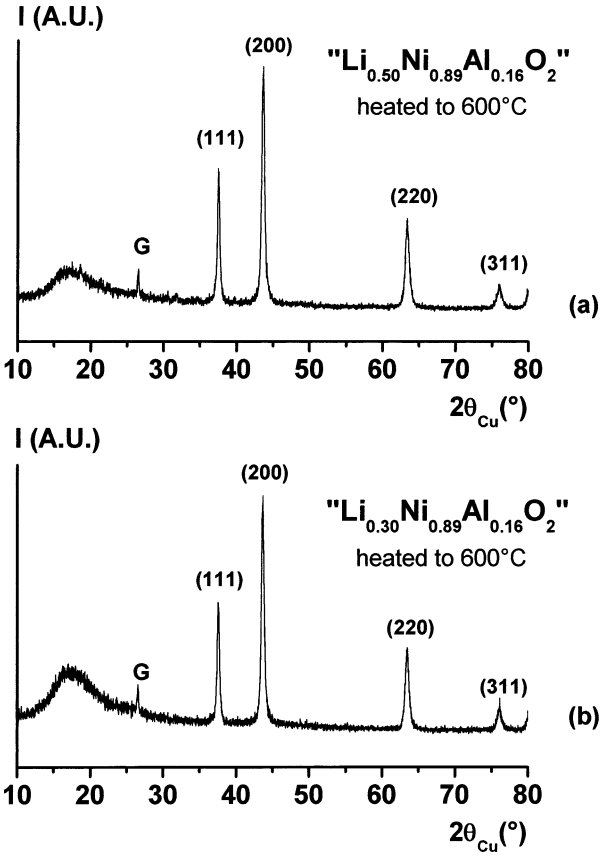

Figure 3. X-ray diffraction patterns recorded for $Li_{0.50}Ni_{0.89}Al_{0.16}O_2$ (a) and $Li_{0.30}Ni_{0.89}Al_{0.16}O_2$ (b) after the TGA/MS experiments (performed up to 600 °C).

Because of the partial ionization of water molecules, the water loss is also observed on the oxygen release curves, which explains the shoulder observed around 240 °C for $Li_{0.50}Ni_{0.89}Al_{0.16}O_2$. The comparison of the oxygen release curves obtained for $Li_{0.50}Ni_{1.02}O_2$ and $Li_{0.50}Ni_{0.89}Al_{0.16}O_2$ (Figure 2a) shows that the oxygen release starts at 265 and 290 °C for these materials, respectively. Note that the results for $Li_{0.50}Ni_{1.02}O_2$ are in good agreement with those reported by Dahn et al. for similar phases.[5]

As shown in Figure 3a for the particular case of $Li_{0.50}Ni_{0.89}Al_{0.16}O_2$, a significant structural modification occurs during heating to 600 °C. Indeed, the XRD patterns of $Li_{0.50}Ni_{1.02}O_2$ and $Li_{0.50}Ni_{0.89}Al_{0.16}O_2$ recovered at the end of the TGA/MS analyses are both characteristic of a NiO-type structure (space group $Fm3m$). The theoretical weight losses corresponding to the structural transition between the initial phase and NiO-type phases are 8.06% and 7.82% for $Li_{0.50}Ni_{1.02}O_2$ and $Li_{0.50}Ni_{0.89}Al_{0.16}O_2$, respectively, according to the global reactions 1 and 2:

$$Li_{0.50}Ni_{1.02}O_2 \rightarrow 1.52\ (Li_{0.33}Ni_{0.67}O) + 0.24\ O_2 \quad (1)$$

$$Li_{0.50}Ni_{0.89}Al_{0.16}O_2 \rightarrow 1.55\ (Li_{0.33}Ni_{0.57}Al_{0.10}O) + 0.225\ O_2 \quad (2)$$

The experimental values obtained for $Li_{0.50}Ni_{1.02}O_2$ (5.6%) and $Li_{0.50}Ni_{0.89}Al_{0.16}O_2$ (6.2%) are somewhat less than the theoretical ones. In reactions 1 and 2, an ideal chemical formula has been assumed for the NiO-type phase. However, it is well-known that at low temperature, materials with cationic vacancies can be obtained, which leads to a smaller oxygen release. For example, the decomposition of β-$Ni(OH)_2$ leads to the formation of NiO_x ($x \approx 1.3$) at 300 °C.[19]

As shown in Figure 4 for $Li_{0.30}Ni_{1.02}O_2$ and $Li_{0.30}Ni_{0.89}Al_{0.16}O_2$, similar thermal behavior is observed for lithium compositions with $x < 0.50$, but with an additional oxygen release occurring at lower temperature (as it appears clearly in Figure 2b, near 190 °C for $Li_{0.30}Ni_{1.02}O_2$ and 215 °C for $Li_{0.30}Ni_{0.89}Al_{0.16}O_2$). For $Li_{0.30}Ni_{1.02}O_2$, the "second" oxygen release occurs in several steps, showing the complex character of the decomposition process that occurs through the formation of several intermediate phases.

Consistent with the results for $x = 0.50$, comparison of the oxygen release curves of $Li_{0.30}Ni_{1.02}O_2$ and $Li_{0.30}Ni_{0.89}Al_{0.16}O_2$ shows that the oxygen release occurs at higher temperatures for the aluminum-substituted compound (Figure 2b). At the end of the thermal process, compounds with NiO-type structures are also obtained from $Li_{0.30}Ni_{1.02}O_2$ and $Li_{0.30}Ni_{0.89}Al_{0.16}O_2$, as shown in Figure 3b for the particular case of $Li_{0.30}Ni_{0.89}Al_{0.16}O_2$. The comparison between the theoretical weight losses, corresponding to the structural transition between the initial phase and the NiO-type phases, and the experimental weight losses determined by TGA, shows a good agreement (respectively 11.56 versus 12.6% for $Li_{0.30}$-

(19) Shirakami, T.; Takematsu, M.; Hirano, A.; Kanno, R.; Yamaura, K.; Takano, M.; Atake, T. *Mater. Sci. Eng.* **1998**, *B54*, 70.

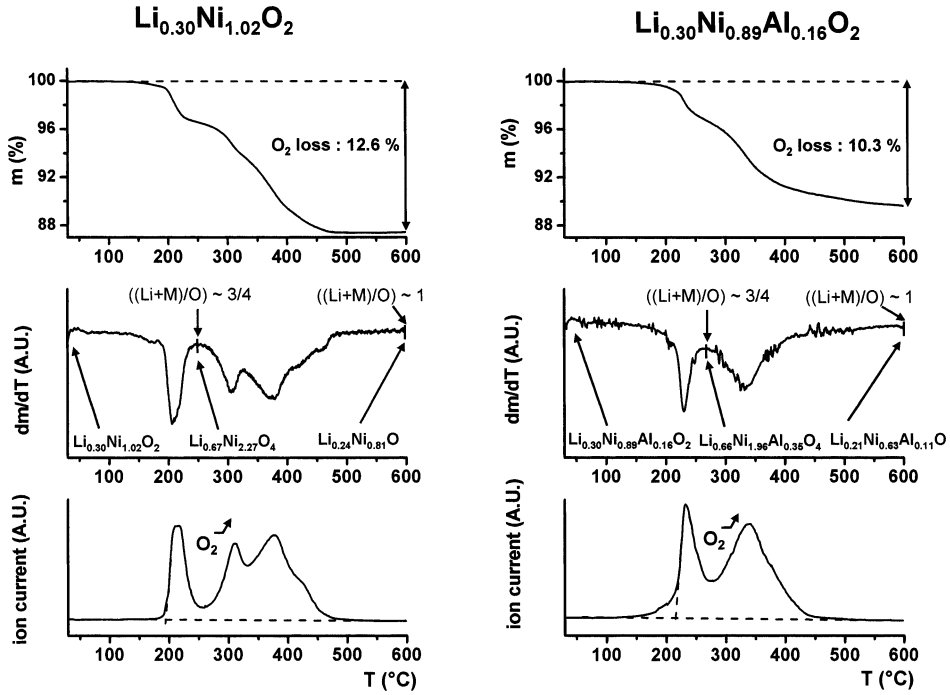

Figure 4. Thermal gravimetric analyses coupled with mass spectrometry for $Li_{0.30}Ni_{1.02}O_2$ and $Li_{0.30}Ni_{0.89}Al_{0.16}O_2$ (sample mass ≈30 mg, heating rate 5 °C/min under an argon stream). The ((Li + M)/O) ratios and chemical compositions are given before and after each oxygen release.

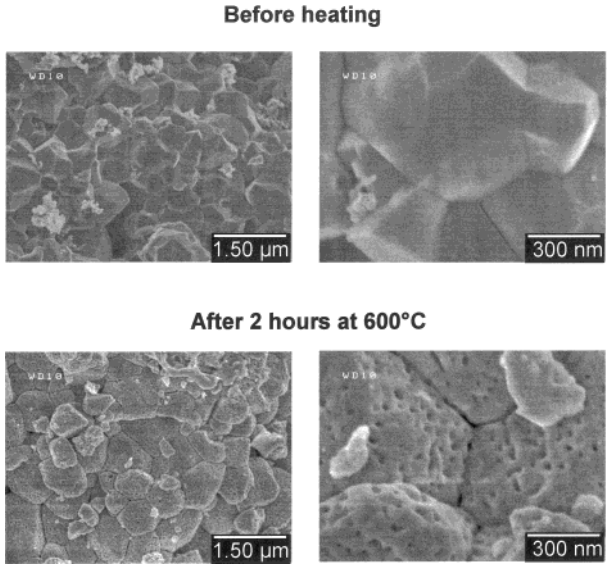

Figure 5. Scanning electron micrographs obtained for $Li_{0.30}Ni_{0.89}Al_{0.16}O_2$ before and after heating at 600 °C for 2 h.

$Ni_{1.02}O_2$ and 11.46 versus 10.3% for $Li_{0.30}Ni_{0.89}Al_{0.16}O_2$), thus confirming the following global reactions:

$$Li_{0.30}Ni_{1.02}O_2 \rightarrow 1.32\ (Li_{0.23}Ni_{0.77}O) + 0.34\ O_2 \quad (3)$$

$$Li_{0.30}Ni_{0.89}Al_{0.16}O_2 \rightarrow 1.35\ (Li_{0.22}Ni_{0.66}Al_{0.12}O) + 0.325\ O_2 \quad (4)$$

Note that in the cases of $Li_{0.30}(Ni,Al)O_2$ compounds, it was not possible to separate the water loss from the first oxygen loss peak. Therefore, the experimental values are slightly overvalued.

The effect of oxygen evolution on the material morphology is clearly observed in Figure 5, which shows the SEM images of the $Li_{0.30}Ni_{0.89}Al_{0.16}O_2$ phases recovered from the battery and after thermal treatment at 600 °C. The general shape of the particles is maintained and the cohesion of the particles is only slightly modified. However, a large number of holes resulting from the oxygen evolution can be observed both in the bulk and in the boundaries between particles.

In situ X-ray Diffraction. The XRD patterns recorded in situ for $Li_{0.50}Ni_{1.02}O_2$, $Li_{0.30}Ni_{1.02}O_2$, $Li_{0.50}Ni_{0.89}Al_{0.16}O_2$, and $Li_{0.30}Ni_{0.89}Al_{0.16}O_2$ deintercalated phases upon increasing temperature are given in Figures 6 and 7. The same type of evolution is observed for the four materials, described as follows. (1) From room temperature to about 150 °C, no structural evolution occurs, and only a slight modification of the cell parameters is observed for $Li_{0.30}Ni_{1.02}O_2$, $Li_{0.50}Ni_{0.89}Al_{0.16}O_2$, and $Li_{0.30}Ni_{0.89}Al_{0.16}O_2$. For $Li_{0.50}Ni_{1.02}O_2$, one can observe that the monoclinic distortion, corresponding to lithium/vacancy orderings in the interslab space and charge (Ni^{3+}/Ni^{4+}) orderings in the slab,[20,21] progressively disappears. This is illustrated in Figure 8, which shows how the $(20\bar{2})$ and (111) diffraction lines of the *C*2/*m* space group merge into the (104) single diffraction line of the $R\bar{3}m$ space group with increasing temperature. (2) From 150 to 180−240 °C (depending on the material), the progressive merging of the (018)/(110) doublet lines is observed. As it will be further discussed, the phases obtained after this first structural transition have XRD patterns characteristic of a spinel structure and can be indexed in the cubic system (space group *Fd*3*m*). (3) At higher temperatures, two-phase domain is observed for $Li_{0.50}Ni_{1.02}O_2$, $Li_{0.30}Ni_{1.02}O_2$, and $Li_{0.30}Ni_{0.89}Al_{0.16}O_2$, leading to the formation of phases which exhibit XRD patterns quite similar to those of NiO-type structures. This

(20) Pérès, J. P.; Weill, F.; Delmas, C. *Solid State Ionics* **1999**, *116*, 19.
(21) Arroyo de Dompablo, M. E.; Marianetti, C.; Van der Ven, A.; Ceder, G. *Phys. Rev. B* **2001**, *63*, 144107.

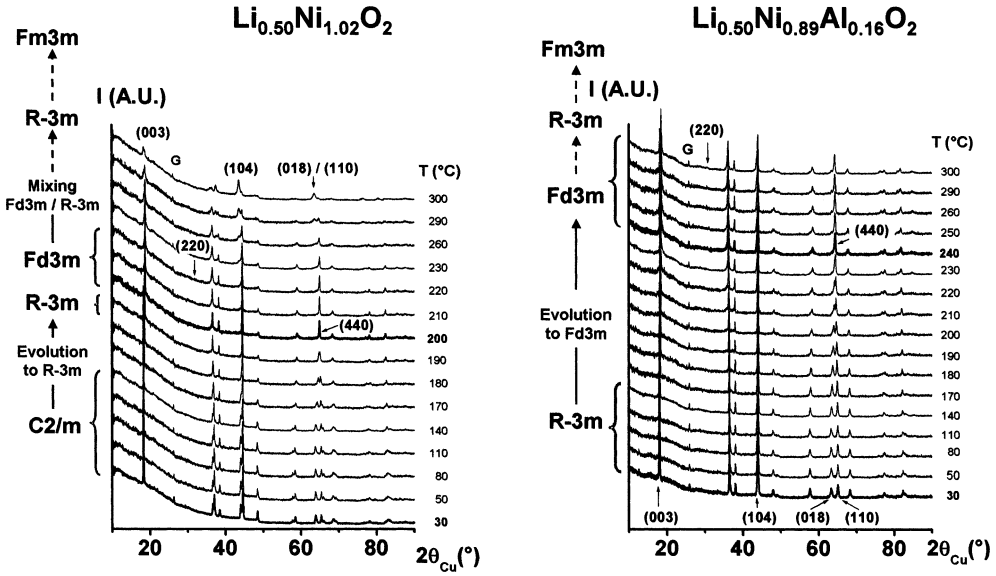

Figure 6. In situ X-ray diffraction patterns of $Li_{0.50}Ni_{1.02}O_2$ and $Li_{0.50}Ni_{0.89}Al_{0.16}O_2$ at increasing temperatures (heating rate 15 °C/min, waiting time before measurement at each temperature step 10 min, data acquisition time 1 h).

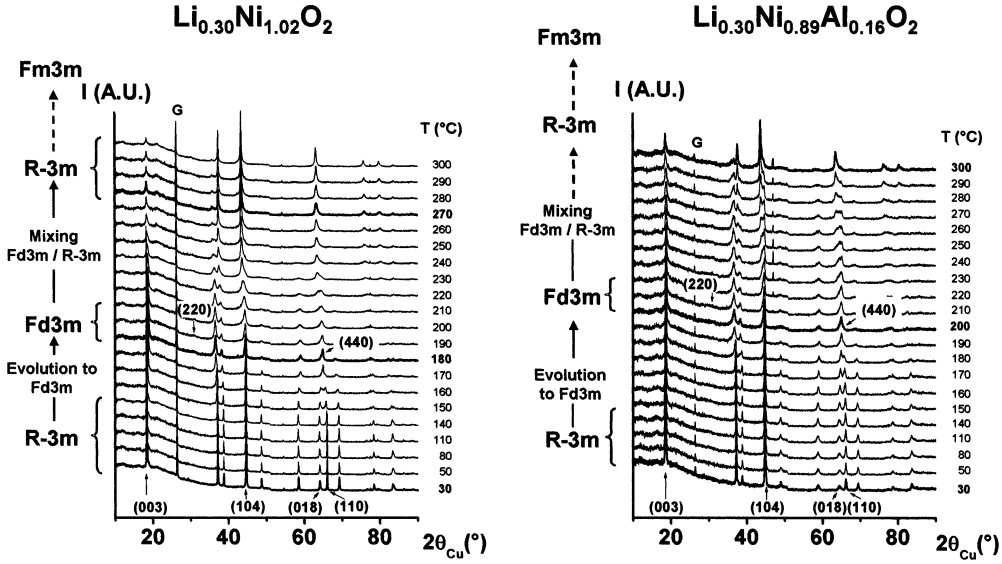

Figure 7. In situ X-ray diffraction patterns of $Li_{0.30}Ni_{1.02}O_2$ and $Li_{0.30}Ni_{0.89}Al_{0.16}O_2$ upon increasing temperature (heating rate 15 °C/min, waiting time before measurement at each temperature step 10 min, data acquisition time 1 h).

second transition is not observed for $Li_{0.50}Ni_{0.89}Al_{0.16}O_2$ (Figure 6) because of the 300 °C temperature limitation of the capillary furnace. However, as shown by the XRD pattern recorded after the TGA measurements, the formation of the NiO-type structure also occurs for this phase, but at temperatures above 300 °C.

To confirm that the materials obtained at the end of the first transition indeed have a spinel-type structure (space group $Fd3m$) and not a disordered $(Li_xNi_z)_{3b}$-$(Ni_{1-y-t}Al_yLi_t)_{3a}O_2$ type structure (space group $R\bar{3}m$), ex-situ XRD patterns were recorded on the $Li_{0.50}Ni_{0.89}$-$Al_{0.16}O_2$ and $Li_{0.30}Ni_{0.89}Al_{0.16}O_2$ phases after heating for 2 h at 240 and 200 °C, respectively. As shown in Figure 9, a better signal/noise ratio was obtained in these analyses. The obvious presence of the (220) diffraction line, characteristic of the $Fd3m$ space group, confirms unambiguously the formation of a spinel-type phase. Indeed, without the presence of the (220) diffraction line, one could also index the XRD patterns in the R$\bar{3}$m space group. "Pseudo-spinel" will be used in the following instead of "spinel" to describe the structural type of these phases because, contrary to the spinel phases that are directly synthesized at high temperature, these phases are obtained through cationic migrations occurring at low temperature and are, therefore, not perfectly ordered. Note that the temperature of these thermal treatments was chosen in agreement with the results obtained from the diffraction experiments performed in situ (Figures 6 and 7). The cell parameter refinements of these ex situ XRD patterns give the following values: $a = 8.0780(3)$ Å for $Li_{0.50}Ni_{0.89}Al_{0.16}O_2$ and $a = 8.0900(5)$ Å for $Li_{0.30}Ni_{0.89}Al_{0.16}O_2$. These are in good agreement with those reported for the $LiNi_2O_4$ spinel phase ($a = 8.041(3)$ Å,[9] $a = 8.087(2)$ Å[22]).

Due to low resolution, large broadening of the diffraction lines, and the presence of parasitic lines corresponding to the capillary furnace, it was not possible

(22) Kanno, R.; Kubo, H.; Kawamoto, Y.; Kamiyama, T.; Izumi, F.; Takeda, Y.; Takano, M. *J. Solid State Chem.* **1994**, *110*, 216.

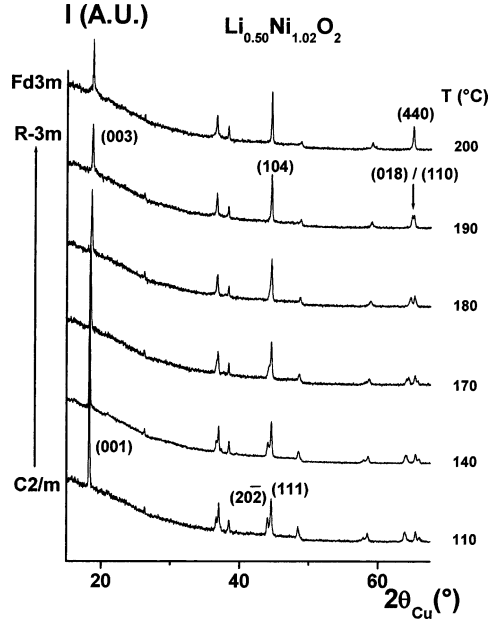

Figure 8. Enlargement of the in situ X-ray diffraction patterns of $Li_{0.50}Ni_{1.02}O_2$, in the [15−67.5° (2θ)] range and between 110 and 200 °C: showing the progressive disappearance of the monoclinic distortion.

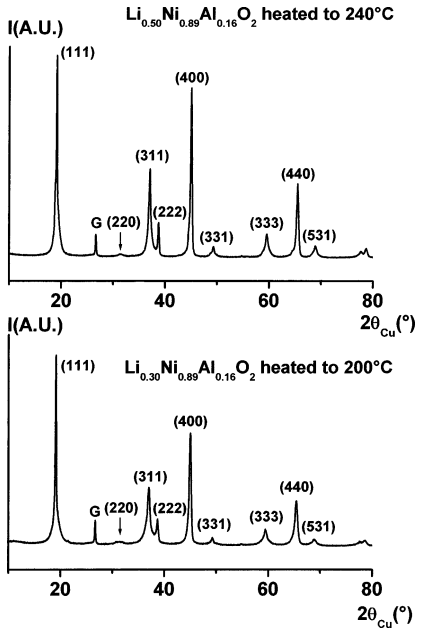

Figure 9. Ex situ X-ray diffraction patterns of $Li_{0.50}Ni_{0.89}Al_{0.16}O_2$ after 2 h at 240 °C and of $Li_{0.30}Ni_{0.89}Al_{0.16}O_2$ after 2 h at 200 °C.

to refine the in situ XRD patterns by the Rietveld method. However, they could be indexed with monoclinic ($C2/m$), hexagonal ($R\bar{3}m$), or cubic ($Fd3m$) cells respectively (as pointed out in Figures 6 and 7). In each case, the hypothetical $a_{hex.}$ and $c_{hex.}$ parameters were deduced from the real cells to allow a general comparison of the various materials. Figure 10 shows the evolution of the $c_{hex.}/a_{hex.}$ ratio versus temperature for the various $Li_x(Ni,Al)O_2$ compounds during the first step of the degradation process (i.e., lamellar to pseudo-spinel transition). A decrease of the $c_{hex.}/a_{hex.}$ ratio with increasing temperature is observed for all compounds. At the end of this first step, the ratio stabilizes around 4.90, which is the theoretical value for a cubic structure,

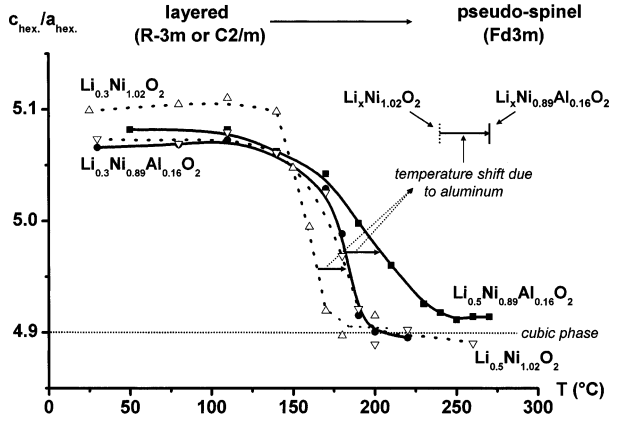

Figure 10. Evolution of the $c_{hex}/a_{hex.}$ ratio versus temperature for $Li_{0.50}Ni_{1.02}O_2$ (-▽-), $Li_{0.30}Ni_{1.02}O_2$ (-△-), $Li_{0.50}Ni_{0.89}Al_{0.16}O_2$ (−■−), and $Li_{0.30}Ni_{0.89}Al_{0.16}O_2$ (−●−). The $a_{hex.}$ and $c_{hex.}$ parameters were calculated from the X-ray diffraction patterns recorded in situ upon increasing temperature.

thus providing additional confirmation of the formation of the pseudo-spinel phase. Note that this thermal transition occurs at higher temperatures for compounds with larger amounts of lithium and/or aluminum.

To summarize, the same type of evolution is observed for the four materials: the structure evolves from a 2D layered structural type to a 3D NiO-type through two steps.

During the first step, which occurs around 150 and 240 °C, depending on the material composition, the progressive merging of the (018)/(110) diffraction lines from the $R\bar{3}m$ space group, associated with the appearance of the (220) diffraction line from the $Fd3m$ space group, indicates a progressive structural transition from the initial lamellar α-$NaFeO_2$-type phase to a "LiM_2O_4" pseudo-spinel-type phase, through a solid solution reaction.

The second step corresponds to the transition, through a two-phase domain, between the "LiM_2O_4" pseudo-spinel phase and a highly disordered phase, which crystallizes in the $R\bar{3}m$ space group. This phase can be considered as an intermediate between the spinel phase and a NiO-type phase. The decrease of the (003)/(104) intensity ratio during this phase transition shows that a Li/Ni(Al) ion exchange occurs between the slab and the interslab space as the temperature increases. Also, with increasing temperature, the disordered $R\bar{3}m$ phase transforms progressively to the NiO-type structure, as shown by the disappearance of the (003) diffraction line. This reaction occurs through a structural reconstruction as a significant amount of oxygen is lost (∼25%). Note that because of the 300 °C temperature limitation of the capillary furnace, it was not possible to follow the complete thermal degradation in situ.

The comparison of the thermal behavior of the four materials shows that the more deintercalated materials are also the more thermally unstable. Indeed, the pseudo-spinel phase is obtained at higher temperature for $Li_{0.50}Ni_{1.02}O_2$ and $Li_{0.50}Ni_{0.89}Al_{0.16}O_2$ (200 and 240 °C, respectively) than for $Li_{0.30}Ni_{1.02}O_2$ and $Li_{0.30}Ni_{0.89}Al_{0.16}O_2$ (180 and 200 °C, respectively). Moreover, for the same lithium content in the structure, aluminum-substituted compounds are more stable, with higher phase transition temperatures and a larger temperature existence range for the pseudo-spinel phase. The pseudo-

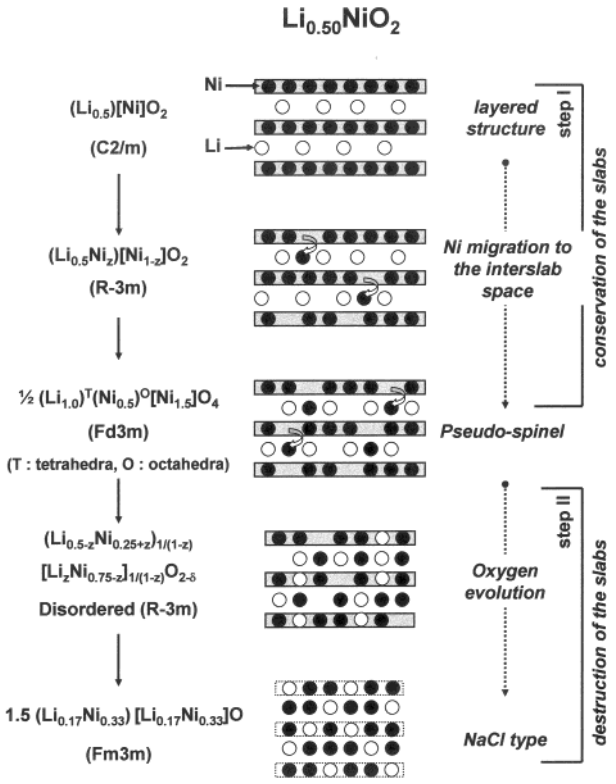

Figure 11. Structural modifications proposed for $Li_{0.50}NiO_2$ during the thermal degradation process.

spinel is completely transformed into the disordered $R\bar{3}m$ phase at 270 °C for the $Li_{0.30}Ni_{1.02}O_2$ composition, whereas the transformation is not completely finished at 300 °C for the $Li_{0.30}Ni_{0.89}Al_{0.16}O_2$ composition.

Note that the differences in temperature observed between the XRD and the TGA/MS experiments are due to kinetic effects. As expected, and as previously shown by Dahn, the oxygen release onset temperature is very dependent on the heating rate.[5] Indeed, oxygen losses appear at lower temperatures for the XRD experiments due to a much slower heating rate (around 20 h is necessary to reach 300 °C) than the rate used for the TGA/MS analyses (5 °C/min: only 55 min is necessary to reach 300 °C).

Discussion

Mechanism. *For the $Li_{0.50}(Ni,Al)O_2$ Compositions.* Figure 11 illustrates the proposed structural evolution during the thermal degradation process in the case of the ideal $Li_{0.50}NiO_2$ phase. The following two steps can be considered. The first step, corresponding to the progressive transition between the lamellar α-$NaFeO_2$-type structure ($R\bar{3}m$ or $C2/m$) and a "LiM_2O_4" pseudo-spinel structure ($Fd3m$), occurs through the overall migration of one-quarter of the nickel cations from the slab to the interslab space and through the displacement of the lithium ions from octahedral to tetrahedral sites in the interslab space. During this first step, the cfc oxygen lattice is preserved and a change in cationic distribution occurs progressively as seen by XRD. An electron diffraction study would be useful to study this transition in more detail at the microscopic level.

The second step, which consists of the transformation of the pseudo-spinel phase into a highly disordered phase (space group $R\bar{3}m$), is associated with a progressive destruction of the slabs due to oxygen departure. Indeed, for the deintercalated materials, the (Li + M)/O initial ratio is always smaller than 1. Therefore, an oxygen release is required in order to reach a (Li + M)/O ratio equal to 1, the theoretical value observed for NiO-type compounds, where all cations are statistically distributed within the octahedral sites of the cfc oxygen lattice.

For the $Li_{0.30}(Ni,Al)O_2$ Compositions. For the $Li_{0.30}(Ni,Al)O_2$ phases, the first step of the degradation mechanism is associated with an oxygen release (Figure 4). Indeed, in the $Li_{0.50}Ni_{1.02}O_2$ and $Li_{0.50}Ni_{0.89}Al_{0.16}O_2$ phases the (Li + M)/O ratio is equal to 3/4, the same theoretical value observed for a "LiM_2O_4" spinel-type phase. In contrast, for the $Li_{0.30}Ni_{1.02}O_2$ and $Li_{0.30}Ni_{0.89}Al_{0.16}O_2$ phases, the (Li + M)/O ratio is smaller than 3/4. Therefore, during the first step, an oxygen release is required even for the lamellar to pseudo-spinel phase transition according to reactions 5 or 6:

$$Li_{0.30}Ni_{1.02}O_2 \rightarrow 0.12\ O_2 + Li_{0.30}Ni_{1.02}O_{1.76} \quad (\approx Li_{0.68}Ni_{2.32}O_4) \quad (5)$$

$$Li_{0.30}Ni_{0.89}Al_{0.16}O_2 \rightarrow 0.10\ O_2 + Li_{0.30}Ni_{0.89}Al_{0.16}O_{1.8} \quad (\approx Li_{0.67}Ni_{1.98}Al_{0.36}O_4) \quad (6)$$

Note that the chemical compositions obtained experimentally from the TGA/MS analyses for the pseudo-spinel phases (as reported in Figure 4) are in excellent agreement with those expected (i.e., $Li_{0.67}Ni_{2.27}O_4$ vs $Li_{0.68}Ni_{2.32}O_4$ and $Li_{0.66}Ni_{1.96}Al_{0.35}O_4$ vs $Li_{0.67}Ni_{1.98}Al_{0.36}O_4$).

During the second step to form NiO-type structures, further oxygen release occurs, as shown by the TGA/MS analyses (Figures 1 and 4).

Relative Stability of the Materials. This thermal study has shown, as expected, that the stability of the delithiated $Li_x(Ni,Al)O_2$ phases decreases with decreasing lithium content. Indeed, upon oxidation (i.e., delithiation), there is formation of an increasing amount of unstable Ni^{4+} ions in the material, which are subsequently reduced back to Ni^{3+} at elevated temperatures with concurrent loss of oxygen.

Furthermore, it appears that an increasing aluminum substitution for nickel induces a decrease in the kinetics of the pseudo-spinel phase formation and a stabilization of this pseudo-spinel phase over a larger temperature range. The lamellar to pseudo-spinel transformation occurring during the thermal degradation process implies cationic migrations between the octahedral sites in the slab and those in the interslab space, via tetrahedral sites, as shown in Figure 12, which represents the theoretical path for the nickel or aluminum ions during the first step of the thermal transformation. The Al^{3+} ions, being highly stable in a tetrahedral environment, probably migrate preferentially versus nickel ions from the slab to the interslab space, to form the pseudo-spinel phase upon increasing temperature. Indeed, due to their d^6 electronic configuration, low spin Ni^{4+} ions are not stable in tetrahedral sites, whereas a nonfavorable low spin to high spin transition is required for Ni^{3+} (d^7) ions to migrate to tetrahedral sites.[9] Furthermore, as shown in Figure 12, in contrast to

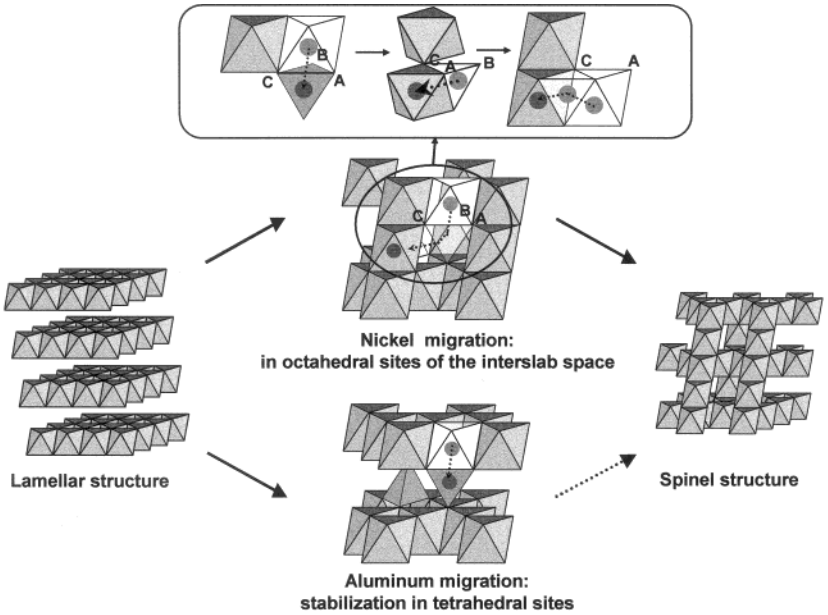

Figure 12. Theoretical path for the nickel or aluminum ions during the lamellar to spinel transition. In the case of aluminum migration, the intermediate structures with aluminum in tetrahedral sites are stabilized, thereby pushing the formation of the pseudo-spinel-type phase to higher temperatures.

nickel ions, the Al^{3+} ions are probably stabilized in the intermediate tetrahedral sites, making the cationic rearrangements necessary for the formation of the pseudo-spinel phase more difficult, thereby decreasing the kinetics of the pseudo-spinel formation. The stability of the aluminum-substituted pseudo-spinel phase increases with an increasing aluminum substitution for nickel, probably for the same reasons. Indeed, during the formation of the NiO-type phase, the tetrahedral sites must be involved even if a local structural reconstruction occurs.

A neutron diffraction study is planned on the high-intensity diffractometer D20 of Institut Laue-Langevin (ILL, Grenoble, France), to confirm this proposed mechanism for the increased stability of the aluminum-substituted lithium nickelate compounds.

Acknowledgment. We thank P. Dagault for thermal analyses, P. Biensan, C. Jordy, and J.P. Pérès for fruitful discussions, and Saft and Région Aquitaine for financial support.

CM030059F